Spectrochimica Acta Part B: Atomic Spectroscopy 198 (2022) 106545

Contents lists available at ScienceDirect

Spectrochimica Acta Part B: Atomic Spectroscopy

journal homepage: www.elsevier.com/locate/sab

Analysis of Zebrafish contamination with heavy metals using a FF-XRF imaging system based on a MPGD

F.D. Leite [a,*], P.M.S. Carvalho [a,b], R.G. Oliveira [a], M.C. Lopes [a], I. Domingues [c], P.M.M. Correia [a], L.F.N.D. Carramate [a], S. Pessanha [b], J.F.C.A. Veloso [a], A.L.M. Silva [a,*]

[a] I3N, Physics Department, University of Aveiro, Campus de Santiago, 3810-193 Aveiro, Portugal
[b] LIBPhys-UNL, Physics Department, NOVA School of Science and Technology, NOVA University Lisbon, Campus Caparica, 2829-516 Monte da Caparica, Portugal
[c] CESAM, Biology Department, University of Aveiro, Campus de Santiago, 3810-193 Aveiro, Portugal

ARTICLE INFO

Keywords:
FF-XRF
X-ray fluorescence imaging
Heavy metals
Danio rerio
THCOBRA

ABSTRACT

Heavy metals have been extensively used by humans and are still present in many aspects of modern-day life. Such elements tend to accumulate, degrading the quality of air, soil, and water, negatively affecting the living organisms. As such, it is of paramount importance to understand the environmental risks of heavy metals, including their bioaccumulation capacity in organisms, since they are associated with several harmful health effects, such as neurological damages. The Zebrafish (*Danio rerio*) has been shown to be an excellent animal model to understand physiological responses in mammals and consequently to perform toxicological studies due to characteristics such as the high genetic and physiological similarity with humans.

In this work, a Full-Field Energy Dispersive X-ray Fluorescence (FF-XRF) imaging system, based on the 2D-THCOBRA micropattern gas detector, was used to monitor heavy metal accumulation in Zebrafish during a water borne exposure bioassay. The distributions of Mn, Se, and Pb in Zebrafish, exposed to different concentrations of the heavy metal compounds during different time intervals, were mapped. The results show a preferential accumulation of Mn, Se, and Pb in the Zebrafish's visceral region and highlight the suitability of the FF-XRF imaging system for quick screening of metal accumulation in fish bioassays.

1. Introduction

Some metals, such as sodium (Na), potassium (K), magnesium (Mg) or calcium (Ca), are essential to the proper functioning of an animal's body [1]. On the other hand, organisms are also exposed to non-essential metals (e.g., lead (Pb) or mercury (Hg)) through environmental pollution (generated by mining, industrial wastewaters, or incorrect treatment of electronic waste, for example) or occupational exposure. If their concentrations exceed pre-defined safety values, they can become toxic. Many of these values have already been studied: for instance, the USA's Centers for Disease Control and Prevention (CDC) has set the standard elevated blood lead level for adults to be 10 μg/dL and for children 5 μg/dL of the whole blood [2]. Still, no known safe blood lead concentration can be considered, as even low concentrations may be associated with several health problems, such as abdominal pain or alterations of the nervous system; in children, lead poisoning is also associated with learning and concentration difficulties [3]. Depending on the level of exposure, some signs and symptoms of heavy metals accumulation can take years to develop as is the case of arsenic (As) poisoning [4]. Manganese (Mn) is essential for intracellular activities, but overexposure may lead to accumulation in the bones, liver, or brain [5], causing several pathologies, e.g., manganism (a disorder that resembles some symptoms of Parkinson's disease) and hepatic encephalopathy, both associated with motor and psychiatric disturbances [6].

Regardless of the acute or chronic exposure to essential and non-essential metals, they are associated with several health problems when their concentrations exceed safe values. Thus, it is necessary to understand the mechanisms of accumulation of metals and the areas/organs where they accumulate depending on their concentration and exposure time, and to comprehend how they may affect the behaviour of living beings. Different animal models have been used to investigate the toxicity of various heavy metals. However, the Zebrafish (*Danio rerio*)

* Corresponding authors.
E-mail addresses: flavia.leite@ua.pt (F.D. Leite), pmd.carvalho@campus.fct.unl.pt (P.M.S. Carvalho), regina.oliveira@ua.pt (R.G. Oliveira), mcarolina.lopes@ua.pt (M.C. Lopes), inesd@ua.pt (I. Domingues), pmcorreia@ua.pt (P.M.M. Correia), laracarramate@ua.pt (L.F.N.D. Carramate), sofia.pessanha@fct.unl.pt (S. Pessanha), joao.veloso@ua.pt (J.F.C.A. Veloso), analuisa.silva@ua.pt (A.L.M. Silva).

https://doi.org/10.1016/j.sab.2022.106545
Received 22 March 2022; Received in revised form 11 October 2022; Accepted 14 October 2022
Available online 18 October 2022

has become the preferred model for in vivo assays [7–9] due to several advantageous characteristics such as the fully sequenced genome, that is 70% homologous to the human genome [10]; and its small size and low maintenance costs. Moreover, fish and mammals present many anatomical and physiological similarities – for example, they have common organs like the brain, heart, intestine, kidney, liver, pancreas, and nervous system [11].

Zebrafish have been extensively used in studies pertaining to the characterization of heavy metal accumulation. Usually, studies are more focused on certain organs through the analysis of biomarkers, and only a small number of studies are dedicated to the evaluation of the elemental concentration and distribution of heavy metals in the whole sample. M. L. Carvalho et al. [12] determined the concentrations of essential and toxic elements in different fish using energy dispersive X-ray fluorescence (EDXRF) and flame atomic absorption spectrometry (FAAS). Bilo et al. [13] studied the accumulation of lead and zinc in Zebrafish embryos using total reflection X-ray fluorescence (TXRF), concluding that XRF analysis was advantageous in determining bioaccumulation and that its application in small-sized organisms might be useful. Korbas et al. [14], using synchrotron X-ray fluorescence mapping, examined the uptake and localization of mercury in Zebrafish larvae, and Leitão et al. [15] used the micro EDXRF technique (μ-EDXRF) to map the distribution of Hg and other trace elements to assess toxicity and bioaccumulation in adult Zebrafish organs.

EDXRF is becoming a standard technique for qualitative and quantitative elemental analysis of different samples, in various fields such as environmental analysis, biological samples' analysis, and study of paintings and other cultural heritage pieces [16–19]. This technique presents many advantages, namely the simultaneous identification of several elements, its non-destructive character (i.e., samples are unaltered after the analysis), and the simple sample preparation [16,18]. Many EDXRF spectrometers also allow mapping the elemental distribution of samples. For example, micro-XRF spectrometer systems scan a desired region of interest, point by-by-point, and register the emitted radiation using a silicon drift detector (SDD) [20].

On the other hand, full-field of view spectrometers can be employed, based on 2D detectors (pixel detectors [21] or gaseous detectors [19]), both position and energy sensitive. Full-field of view systems have the advantage of requiring less analysis time compared to scanning systems, especially on large area samples; they are also less complex and can be manufactured at a fraction of the cost of scanning systems based on SDDs. In this work, we highlight full-field imaging systems based on micropattern gas detectors, such as the Micro-Hole and Strip Plate (MHSP) [19] and the 2D-THCOBRA [22], because of the detectors' advantageous characteristics, such as the absence of background due to the electronic noise by setting a threshold, high-rate capability (> 1 MHz/mm^2), room temperature operation and low cost [23]. Conversely, pixel detectors like CCDs show good position and energy resolution, but present higher complexity of the system for imaging readout and multi-pixel events can occur, which can lead to distortions in the energy spectrum [24].

Silva et al. [19] carried out work with an EDXRF imaging spectrometer based on a Micro-Hole and Strip Plate (MHSP) gas detector. The detector has a 75 μm thick Kapton window with an area of 3 × 3 cm^2. The energy resolution calculation yielded values of 14% at 8 keV, whilst position resolution values as low as 50 μm could be achieved. The system capabilities for biomedical applications were evaluated by measuring the drift of the major constituents of a dental amalgam throughout restored teeth.

Silva et al. [22] proposed an imaging system with an active area of 10 × 10 cm^2, based on a THCOBRA structure, an ionizing radiation source, and a pinhole camera. The detector operates with a gas mixture of Ne/CH_4 (95/5) in continuous flow, and is sensitive to the position and energy of incident photons, which allows mapping the sample. It has a detection efficiency of about 75% at 5.9 keV, an energy resolution of approximately 1 keV FWHM at 5.9 keV, and position resolution values of 400 μm FWHM. This system was used to investigate the elemental distribution of pigments in a contemporary Indian miniature, and later, it was used by Carvalho et al. [25] to analyse and map decorative glazed ceramic pieces.

In this work, the FF-XRF spectrometer based on the 2D-THCOBRA was employed to investigate heavy metal accumulation in Zebrafish during a water borne exposure bioassay. The distribution of Mn, Se, and Pb in different Zebrafish specimens was mapped with the aforementioned spectrometer and validated with the M4 TORNADO. Hence, the suitability of the FF-XRF system based on the 2D-THCOBRA for biomedical applications was verified.

2. Materials and methods

2.1. Zebrafish assay

For the purposes of this study, Zebrafish (*Danio rerio*) maintained at the bioterium of the Biology Department of University of Aveiro (Aveiro, Portugal), were used. The specimens were kept under controlled environmental conditions in a ZebTEC recirculating system: culture water was obtained by reverse osmosis and activated carbon filtered tap water, adjusted for a pH level of 7.5 ± 0.5, temperature of 27 ± 1 °C, and dissolved oxygen saturation ≥ 95%; a photoperiod of 12 h light and 12 h dark was defined.

A total of 12 adult Zebrafish (eight to ten months old) were selected for the experimental assay: 3 sets of 3 specimens were exposed to different contaminants (82 mg/L of manganese sulphate monohydrate – $MnSO_4 \bullet H_2O$, 15.8 mg/L of selenium metal powder - Se, and 3 mg/L of lead sulphate – $PbSO_4$), and an additional set of 3 specimens was added to a controlled clean water treatment. The heavy metal compounds were available in powder form and were diluted in the water of the Zebrafish environment. The concentrations were chosen considering reported values that showed behavioural effects on zebrafish, and also, each metal's lethal concentration [26]–[28].

During the assay, semi-static conditions were maintained, i.e., every five days the media were renovated; the fish were fed, daily, with commercial dry food (Gemma Micro 500), and the mortality rate was monitored.

The acute bioassay, represented in Fig. 1, had a duration of 12 days, with 3 sampling points after 5, 10, and 12 days of heavy metal exposure. At each sampling point, 1 fish was removed from each medium, euthanized by anaesthetic overdose (tricaine methanesulfonate – MS222), snap-frozen at −80 °C, and freeze-dried for 56 h. After sample preparation, for EDXRF analysis, each Zebrafish was glued onto a Mylar film and placed on a sample holder. Thus, a total of 4 specimens were analysed at each sampling point.

2.2. EDXRF imaging systems

2.2.1. Full field-XRF system based on a gaseous detector

The FF-XRF imaging system based on a gaseous detector consists of

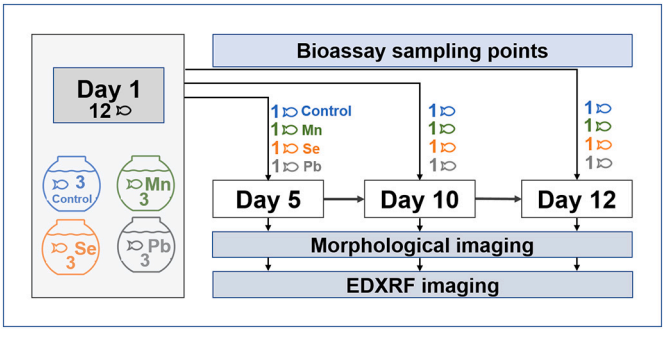

Fig. 1. Experimental design of the heavy metal exposure bioassay.

an X-ray tube with a molybdenum (Mo) anode (series 5000 Apogee from Oxford Instruments), a pinhole camera attached to a stainless-steel structure covered with a lead foil, and a 2D-THCOBRA detector, as shown in Fig. 2. The working principle of this system relies on the irradiation of the whole sample simultaneously. The originated characteristic radiation photons are emitted isotropically, but only the photons that go through the pinhole aperture are detected with the THCOBRA based detector.

The THCOBRA is a Micropattern Gaseous Detector (MPGD) capable of recording both the energy and the position of interaction of each incident photon. Thus, it is suitable for the identification and mapping of the distribution of elements present in the studied samples. The 2D-THCOBRA structure consists of a PCB board made of a 0.4 mm thick G10 plate, coated with a 50 μm copper layer on both sides and it is responsible for the charge multiplication (detector gain) and signal readout. It exhibits a pattern of round holes in an hexagonal geometry in the whole active area (10×10 cm^2) similar to other MPGDs concepts (e.g., Gas Electron Multiplier - GEM or Thick GEM (THGEM)), and a pattern of tops electrodes, orthogonal to the anodes and cathodes electrodes, on the top and bottom face of the structure, respectively [29].

The detector's working principle is based on the interaction of X-ray photons with the filling gas, that leads to ionization and consequent production of ion-electron pairs. Due to an electric field in the drift region, these electrons are directed towards the structure's holes, where the first stage of charge multiplication is induced by a voltage difference applied between the top and cathode electrodes. A second charge multiplication stage occurs in the vicinity of the anode strips, as a voltage difference is applied between the cathode and anode electrodes [29]. The bulk of the generated electric charge is finally collected at the anode strips.

One of the main features of the THCOBRA is the ability to not only determine the energy of the incident photons, but also the corresponding position of interaction. For that, two resistive lines are used, one for each dimension, X and Y, each connecting the anode and the top electrodes, respectively. The induced charges on the electrodes are read at both ends of each resistive line, and the interaction position is determined according to the principle of resistive charge division, in which a signal generated closest to one end of the resistive line will produce a higher amplitude signal at that end than the other end. The energy of each incident photon is determined by summing the signals at the ends of a single resistive line.

A thorough description of the THCOBRA structure can be found on works by Silva et al. [30] and Carramate et al. [31].

2.2.2. Image acquisition and processing parameters

The analysis of the samples was carried out with the FF-XRF system operating in a continuous flow of Ne/CH4 (25 mL/min), and a 500 μm diameter pinhole was used. Acquisition parameters are shown in Table 1. Acquisitions were performed on different days, so it was necessary to adjust the voltage difference between the electrodes to obtain similar gains.

Data acquired from the FF-XRF spectrometer was processed with fluoRADIX, a dedicated software based on MATLAB, thoroughly described in [32]. The software allows visualizing the fluorescence spectrum associated with the sample and the intensity map of the sample, and selecting energy ranges of interest, thus obtaining RGB images where only the corresponding photons are represented.

Table 1
Acquisition parameters: voltage difference applied between the anode and cathode electrodes (V_{AC}) and the cathode and top electrodes (V_{CT}); voltage (V) and current (I) of the X-ray tube; acquisition time (t_a); sample magnification (M).

	V_{AC} (V)	V_{CT} (V)	V (kV)	I (μA)	t_a (min)	M
Mn	185	650	45	450	120	6
Se	180	610	40	336	105	5.2
Pb	195	610	45	362	100	6

It must be noted that the output images present some background noise and pixelization, that may hinder the correct discrimination of features within the samples. As such, a simple image processing algorithm, based on MATLAB, was developed to remove background noise and smooth pixelation. It consists on converting the original image to a greyscale one, to which a contrast adjustment is applied. Then, a mask is created by converting the greyscale image to a matrix of ones and zeros (binary image). The reconstructed image is obtained by multiplying the mask by the original image, which was previously filtered with a median filter. Finally, the morphological image is overlaid on the reconstructed image. This process is shown in Fig. 3.

2.2.3. Limits of detection

Limits of Detection (*LoD*) of the FF-XRF spectrometer, for the analysed elements, were determined as:

$$LoD\ (\mu g/g) = 3c_i\frac{\sqrt{N_B}}{N_P}$$

where c_i is the elemental concentration; N_B is the background peak count rate; and N_P the net peak count rate [33].

The *LoDs* for the analysed elements are presented in Table 2.

The relatively high limits of detection, when compared to spectrometer systems based on solid state detectors, are in line with the detection efficiency of a gas detector filled with Ne/CH_4 [23]. In the case of Se and Pb, the detection efficiency is lower for the energy ranges of the corresponding emission lines, thus decreasing count rates and *LoDs*. Still, in the presented study, the elemental distributions were successfully mapped, with the identified regions of Se and Pb accumulation confirmed with maps obtained with the benchtop spectrometer M4 TORNADO (shown in sections 3.1.2 and 3.1.3).

2.2.4. Micro-XRF - M4 TORNADO

To validate the results obtained with the experimental FF-XRF imaging system, the M4 TORNADO system (Bruker®, Germany), a commercial micro-XRF spectrometer, was used. It is an imaging spectrometer based on scanning, where a region of interest (ROI) of the sample is irradiated point by point with a micro-focused X-ray beam.

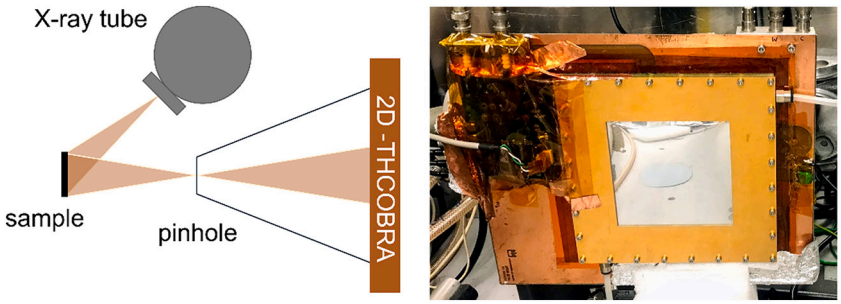

Fig. 2. Left: schematic representation of the FF-XRF spectrometer. Right: photograph of the 2D-THCOBRA based detector.

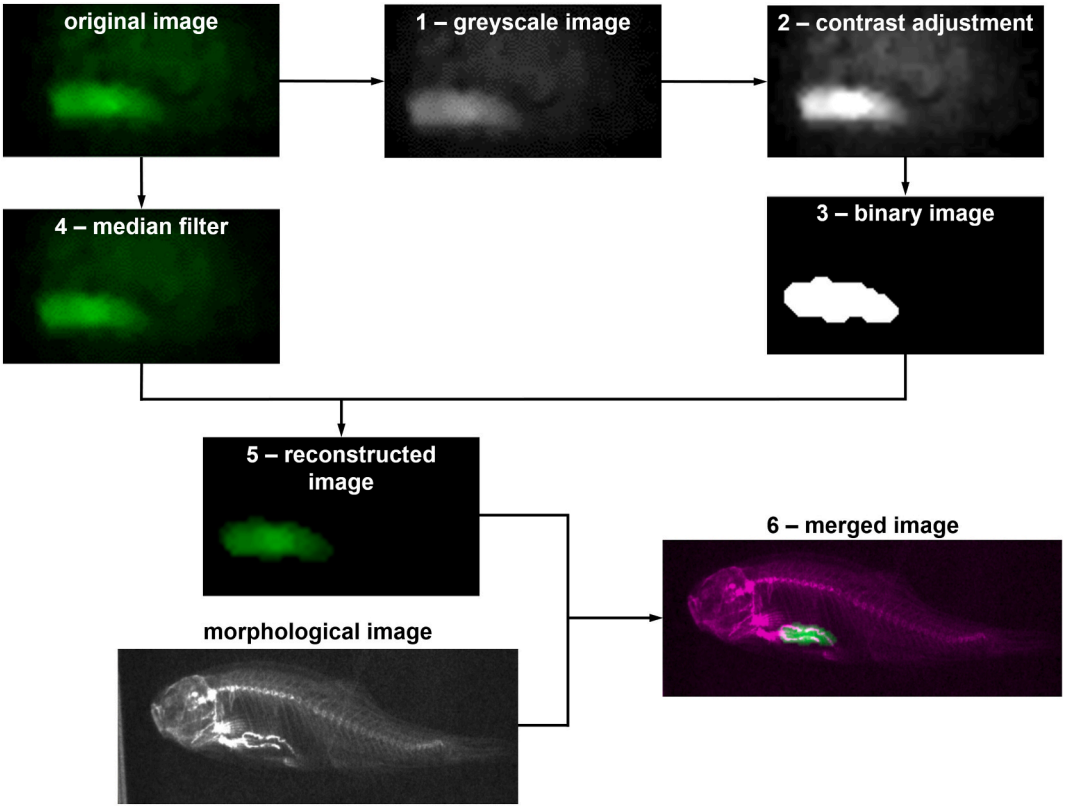

Fig. 3. Image processing algorithm.

Table 2
Limits of Detection for the analysed elements.

Element	LoD ± Δ (μg/g)
Mn	70 ± 6
Se	120 ± 10
Pb	95 ± 10

The M4 TORNADO uses an X-ray tube with a rhodium (Rh) target (operated at 50 kV, 400 μA) to excite the samples, and a polycapillary is used to achieve a spot size down to 25 μm for Mo-Kα radiation. The fluorescence radiation is detected by an energy dispersive silicon drift detector (SDD) with a 30 mm^2 sensitive area and an energy resolution of 142 eV for Mn-Kα (5.9 keV).

Elemental mappings were performed under vacuum (20 mbar), using a composition of filters (100 μm Al/50 μm Ti/25 μm Cu) at the X-ray tube's output to reduce background, and with a lateral step size of 35 μm and time per pixel of 10 ms, resulting in a total measurement time of about 80 min for the analysed samples.

2.3. Morphological images of Zebrafish

Morphological images of the various Zebrafish were acquired with a digital radiography system, composed of an X-ray tube (Castellini Victory X 50), commonly used in dental clinics, and an X-ray image detector based on CMOS technology from Hamamatsu® (S11685–12). The specimens were analysed under the same experimental conditions: exposure time was of 1 ms, and the images were acquired without magnification, with a distance source-detector of 48 cm.

The radiographs of each Zebrafish were overlayed with the

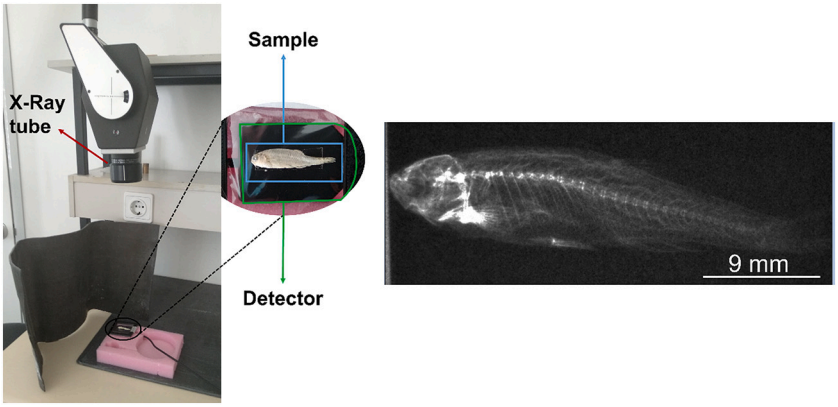

Fig. 4. Left: Photography of the experimental setup of the morphological imaging system. Right: morphological image of a Zebrafish from the control group, sampled after 10 days.

corresponding elemental distribution maps, obtained with the FF-XRF spectrometer, to precisely assess the region of heavy metal accumulation. In Fig. 4, a radiograph of a Zebrafish belonging to the control group is shown, where regions of high density corresponding to the skeletal frame are identified.

3. Results and discussion

Samples of Zebrafish exposed to different heavy metals were analysed with the FF-XRF spectrometer, to identify the elements present in the Zebrafish organism (e.g., Ca and Zn) and to determine if and where heavy metals (Mn, Se, and Pb) accumulate. To validate the results, the specimens were analysed with the micro-XRF M4 TORNADO spectrometer. Moreover, radiographs of all Zebrafish were obtained to precisely determine the regions of accumulation.

3.1. Elemental mapping of heavy metals in Zebrafish

Results of the analysis of the different Zebrafish showed an increased manganese accumulation over time; in the case of selenium, there was also a continuous accumulation of the metal over the course of the assay, but after only 5 days of exposure its accumulation was unequivocally observed. Regarding lead, there was a significant accumulation after 5 days, which became more evident after 12 days. Still, the spatial distribution of lead was similar at all sampling points.

In this section, results are presented for Zebrafish exposed to 82 mg/L of manganese for 12 days, to 15.8 mg/L of selenium for 5 days, and to 3 mg/L of lead for 10 days.

3.1.1. Manganese

Fig. 5 shows the results from the analysis of a zebrafish exposed to 82 mg/L of Mn for 12 days, with the FF-XRF system, and Fig. 6 shows the overlay of the morphologic image with the manganese distribution map. The EDXRF spectrum, the individual spatial distributions of manganese, calcium, and zinc in the zebrafish, and the combined elemental distributions of calcium with manganese, and of calcium and zinc are presented in Fig. 5. Three characteristic peaks are identified on the spectrum, that match the characteristic X-ray peaks of calcium, manganese, and zinc. If the energy ranges of these elements are selected, the corresponding distribution maps are obtained. The distribution of calcium is observed to be uniform over the fish body, being the main constituent of the skeleton and fins, and zinc showed the highest concentration in the eye area, as reported in other works [14,15]. As for manganese, it is possible to see its accumulation in a small area of the visceral region, which is validated by the mapping obtained with the M4 TORNADO spectrometer, shown in Fig. 7. The mappings shown in the Fig. 7 also confirm the higher Zn concentration in the eye as well as the presence of Mn and Zn throughout the specimen, but in lower concentrations.

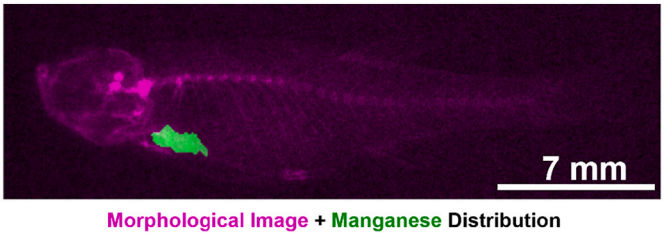

Fig. 6. Overlay of the morphological image of the Zebrafish exposed to Mn (pink) with the elemental distribution map of Mn (green). (For interpretation of the references to colour in this figure legend, the reader is referred to the web version of this article.)

Manganese (Mn) is an essential metal for organisms, however, overexposure to it can cause serious neurological damages as it accumulates in the brain [34,35]. In fact, several studies indicate that zebrafish exposed to manganese show behavioural changes that can be related to the accumulation of the metal in the brain [26,36–38]. Altenhofen et al. [26] conducted a study where adults and larvae Zebrafish were exposed to $MnCl_2$, during 4 and 5 days, respectively, with concentrations ranging from 0.1 mM to 1.5 mM. The results have shown, for example, that exposure to these concentrations lead to alterations in distance travelled or motion time compared with a control group. Bakthavatsalam et al. [36] used zebrafish larvae from 3.5 days

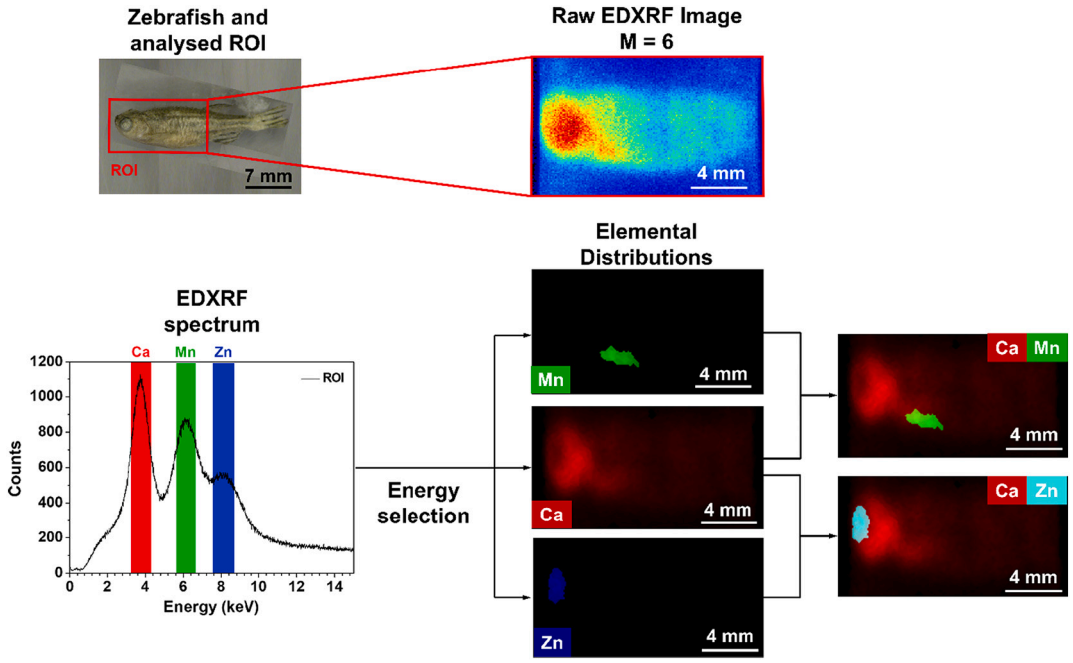

Fig. 5. Results from the analysis of the Zebrafish exposed to Mn during 12 days, with the FF-XRF imaging spectrometer: fluorescence spectrum, raw intensity map, and distribution maps of calcium (red), manganese (green) and zinc (blue). (For interpretation of the references to colour in this figure legend, the reader is referred to the web version of this article.)

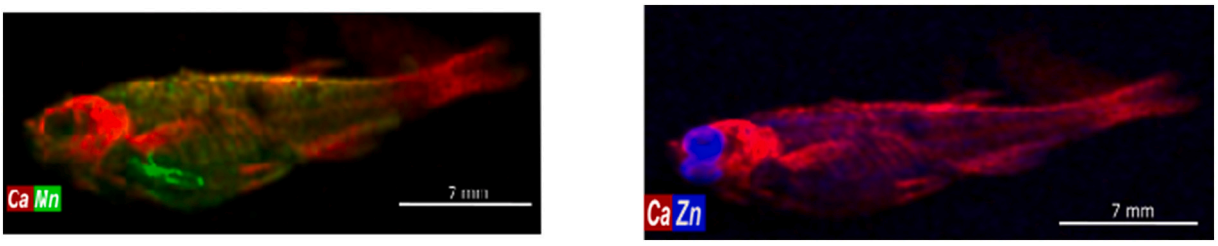

Fig. 7. Elemental maps of the zebrafish exposed to Mn, obtained with M4 TORNADO. Left: calcium (red) and manganese (green); right: calcium and zinc (blue). (For interpretation of the references to colour in this figure legend, the reader is referred to the web version of this article.)

post-fertilization that were treated with $MnCl_2$ in concentrations below 2 mM during 48 h, to assess morphological and behavioural effects of Mn exposure. Defects such as underdevelopment of swim bladder or a tendency to float sideways in comparison with the control group were observed; postural abnormalities and impaired swim motor patterns were exhibited by the Mn-treated larvae. Contrary to these reports, our results showed no accumulation in the brain, which may be due to a) the use of a different Mn compound ($MnSO_4 \bullet H_2O$ instead of $MnCl_2$) in a lower concentration; or b) the different duration of the bioassay. The accumulation in the visceral area could be because this area contains the organs (e.g., liver) involved in the excretion of xenobiotics [39].

3.1.2. Selenium

Selenium (Se) is an essential trace element but at elevated levels becomes toxic. For instance, its excessive intake can lead to gastrointestinal disturbances and neurological diseases [40]. In fish, elevated Se levels manifest through developmental abnormalities or ocular problems, for example. Concerning the accumulation of the metal in zebrafish, it's reported the preferential accumulation in the eye lens' of zebrafish larvae [27,41].

Here, results from the analysis of a zebrafish exposed to 15.8 mg/L of Selenium metal powder for 5 days are presented. It must be noted that during the assay, the Se powder did not dissolve completely in water, and precipitation was visible on the bottom of the aquarium. As such, small Se particles may have been ingested by the zebrafish.

Results from the analysis with the FF-XRF spectrometer are presented in Fig. 8. In the fluorescence spectrum, no peak corresponding to the fluorescence energy of Se (Kα ≈11.2 keV) stands out. However, if the corresponding energy range is selected, the distribution mapping is obtained and accumulation of the metal in the visceral area of the fish is verified. Also, in the raw image, higher intensity is visible in that area. If this high intensity area is selected, the area sum spectrum of the visceral region of accumulation is obtained, and it is possible to identify more clearly a peak corresponding to the Se Kα fluorescence energy (Fig. 9). In the morphological image (Fig. 8), a region of high density is observed (highlighted by the red circle) in the visceral area, corresponding to the region of Se accumulation. This confirms the hypothesis that the fish ingested Se particles that did not fully dissolve, not excreting them

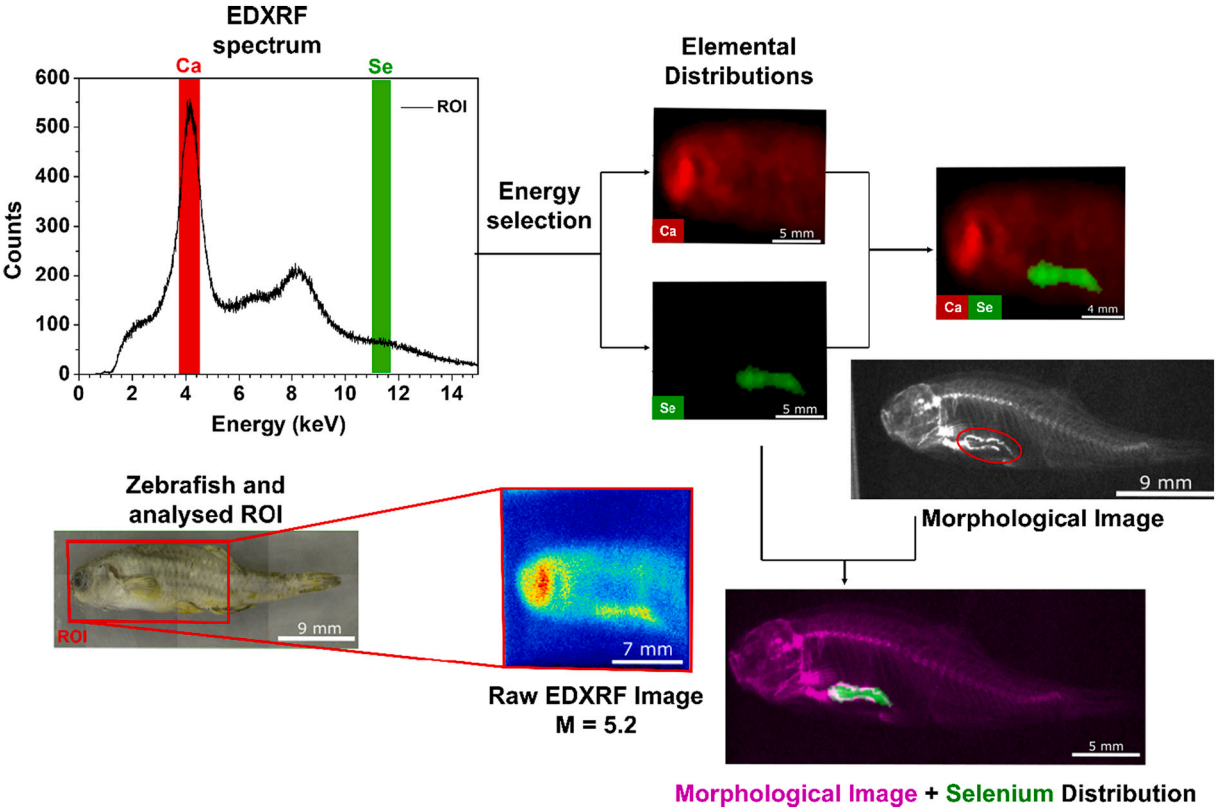

Fig. 8. Results from the analysis of the Zebrafish exposed to Se during 5 days, with the FF-XRF imaging spectrometer: fluorescence spectrum, raw intensity map, distribution maps of calcium (red) and selenium (green), and overlay of the morphological image of the Zebrafish exposed to Se (pink) with the elemental distribution map of Se (green). (For interpretation of the references to colour in this figure legend, the reader is referred to the web version of this article.)

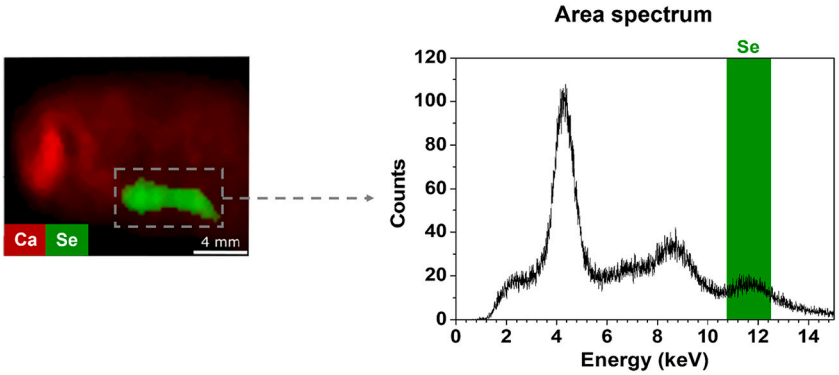

Fig. 9. Visceral region of Se accumulation and corresponding area sum spectrum.

during the assay. The image acquired with the M4 TORNADO, shown in Fig. 10, confirms the preference of selenium accumulation in the visceral area, validating the results obtained with the FF-XRF system.

3.1.3. Lead

Lead (Pb) is one of the most toxic nonessential heavy metals, having been associated with a wide range of harmful effects in humans and animals. Lead poisoning affects the development of children's nervous system, causing irreversible damage [42]. Studies on Zebrafish embryos and adult specimens indicate its negative effect on their behaviour, such as an increase in stress and anxiety levels, for example [43–45]. Pb accumulation is expected to be found in the gills as they are in constant contact with contaminated water, and also in the brain and intestines as predicted by Zhang [46].

In this work, zebrafish were exposed to a concentration of 3 mg/L of Pb for 12 days, with 3 sampling points, to determine the region where lead preferentially accumulates. It was verified that the distribution of lead in all the analysed specimens was more or less constant, i.e., lead accumulated in a similar area of the visceral region. Here, a more detailed elemental analysis is shown after 10 days of exposure to the contaminated medium.

The results obtained with the FF-XRF spectrometer, and the morphological image of the exposed Zebrafish are shown in Fig. 11. A high intensity peak, corresponding to the K energy range of Ca is present on the EDXRF spectrum, whilst no peaks corresponding to the Pb fluorescence peaks are observed. However, if an energy range around the Lα energy (≈10.5 keV) is selected, the Pb distribution map is obtained and shows no trace of metal accumulation in the gills; no accumulation was detected in the brain either, contrasting with the outcomes of Zhang [46]. Still, accumulation in the intestinal region was verified in the analysis with both systems, the FF-XRF and M4 TORNADO, as can be seen in Fig. 11 and Fig. 13. Moreover, the selection of the accumulation area gives rise to an area sum spectrum where a small peak corresponding to the Lα fluorescence energy of Pb can be identified, as shown in Fig. 12.

By merging the image of lead distribution in the zebrafish with the morphological image, the accumulation of this metal in the visceral area was verified. Fig. 13 shows the elemental maps acquired with the M4 TORNADO, that confirm the presence of lead in the zebrafish and its accumulation in the visceral region.

With the M4 TORNADO system, it is also possible to observe lower accumulation of calcium in the operculum area. This small feature is harder to identify with the FF-XRF system, because of its worse position resolution, but it still can be inferred from the Ca intensity profile along the length of the Zebrafish and from the 3D intensity map, both shown in Fig. 14. When the operculum area is selected in the calcium intensity map, a sharp decrease in intensity is observed corresponding to the lower concentration of calcium. The 3D intensity map highlights the intensity gap in the operculum area.

This indicates the potential of the experimental system for analyses where it may be necessary to map samples in more detail.

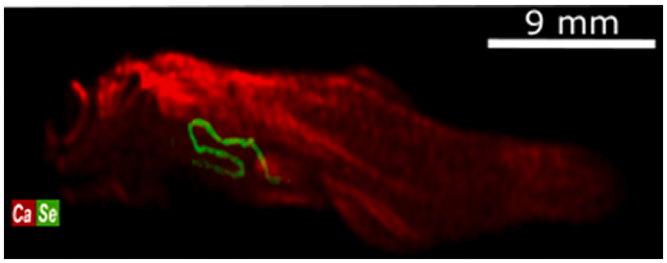

Fig. 10. Elemental map of the zebrafish exposed to selenium, acquired with M4 TORNADO. Calcium is shown in red and selenium in green. (For interpretation of the references to colour in this figure legend, the reader is referred to the web version of this article.)

4. Conclusions

In this work, a bioassay was conducted, in which Zebrafish were exposed to elevated concentrations of Mn, Se, and Pb, to monitor heavy metal accumulation through elemental distribution mapping. An experimental FF-XRF imaging system, based on the 2D-THCOBRA micro-pattern gas detector was employed for this purpose, having the obtained results been validated with a commercial spectrometer, the micro-XRF system M4 TORNADO.

We have verified the suitability of the FF-XRF imaging system based on the 2D-THCOBRA for detecting and mapping the accumulation of different heavy metals on zebrafish. Zebrafish were exposed to 3 contaminants for 12 days with 3 sampling points and the results obtained for exposures of 12 days for Mn, 5 days for Se and 10 days for Pb are shown. The results of the FF-XRF system clearly show the accumulation of Mn, Pb and Se on the visceral region.

Comparing the two systems used, FF-XRF and micro-XRF (scanning system), it can be seen that the latter shows higher position and energy resolution – 25 μm for Mo-kα vs 400 μm FWHM @ 5.9 keV, and 142 eV vs 1 keV FWHM @ 5.9 keV, respectively. However, it can present limitations regarding, for example, sample size (e.g., when using a system with a closed and unalterable geometry, such as the M4 TORNADO, only samples with areas up to 360 mm × 260 mm can be analysed), scanning complexity (use of expensive optical components, such as pollycapillaries, to focus the X-ray beam for localized irradiation, scanning mechanisms to cover the entire region of analysis), increased acquisition time for large area samples, and large quantities of data to store and analyse. Moreover, semiconductor detectors (such as silicon drift detectors) are quite costly, further increasing the total cost of the system – in the case of the M4 TORNADO, hundreds of k€, versus the more cost-effective FF-XRF system based on the THCOBRA detector (estimated at less than tens

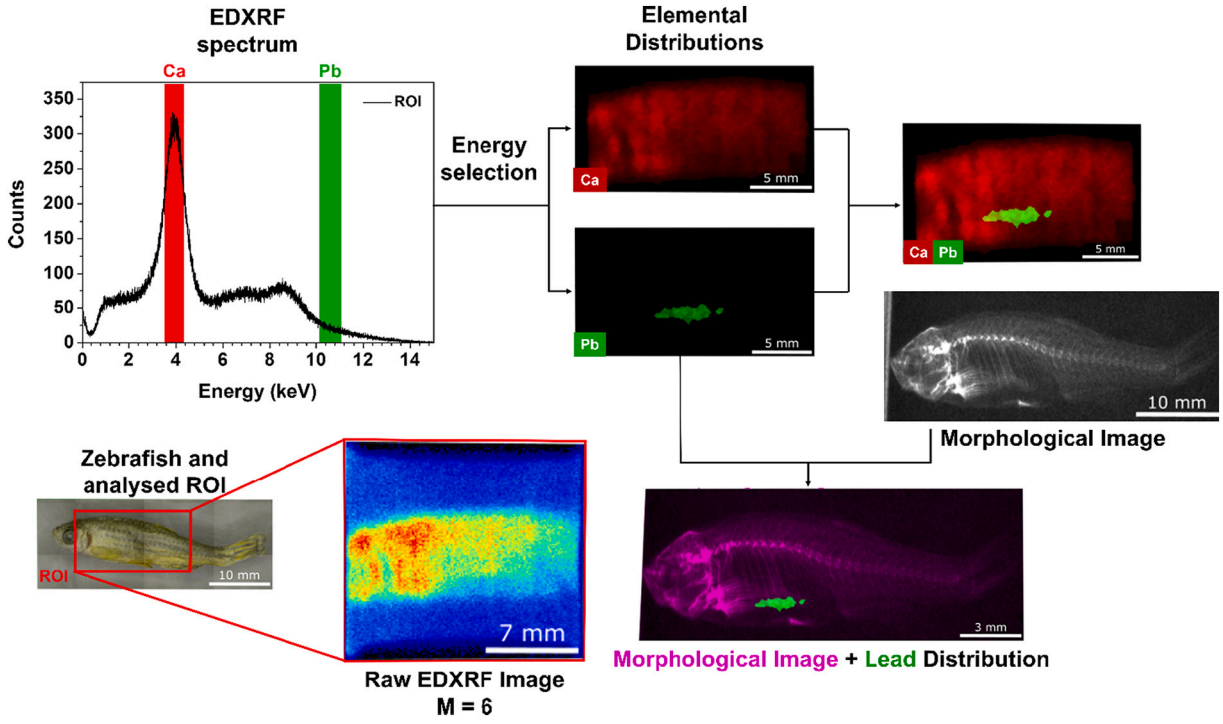

Fig. 11. Results from the analysis of the Zebrafish exposed to Pb during 10 days, with the FF-XRF imaging spectrometer: fluorescence spectrum, raw intensity map, distribution maps of calcium (red) and lead (green), and overlay of the morphological image of the Zebrafish exposed to Pb (pink) with the elemental distribution map of Pb (green). (For interpretation of the references to colour in this figure legend, the reader is referred to the web version of this article.)

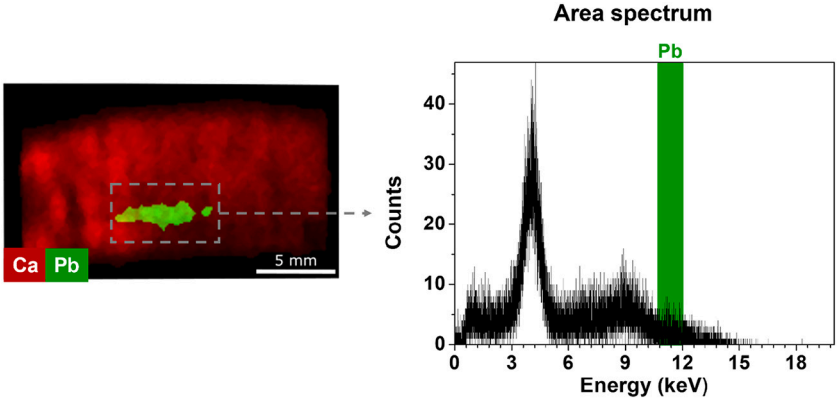

Fig. 12. Visceral region of Pb accumulation and corresponding area sum spectrum.

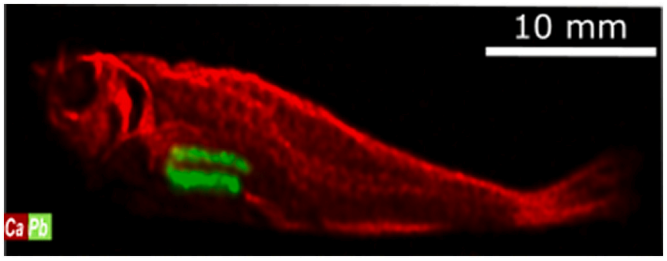

Fig. 13. Elemental map of the zebrafish exposed to Pb, obtained with M4 TORNADO. Calcium is shown in red and lead in green. (For interpretation of the references to colour in this figure legend, the reader is referred to the web version of this article.)

of k€). The presented FF-XRF system allows obtaining qualitative information on the elemental distribution in samples, with short acquisition times and without restriction on the size and appearance/type (rough and/or irregular surface) of the sample. It must also be noted that the performance (e.g., detection efficiency, position resolution) of the THCOBRA-based system can be improved with different filling gases, such as heavier pure noble gases (e.g., krypton or xenon) or mixtures of such gases [22,23].

Despite the apparent limitations of the FF-XRF spectrometer based on the 2D-THCOBRA gas detector, we verified that the elements of interest (Ca, Zn, Mn, Pb, and Se) are detected and the corresponding elemental distribution maps are obtained with enough detail to identify the region of accumulation and features of the specimens' body. For instance, a higher concentration of Zn in the Zebrafish's eye was determined, as well as lower Ca concentration in the operculum. Moreover, the acquisition time was similar for both spectrometers, 100–120 min for the FF-XRF system and about 80 min for the M4

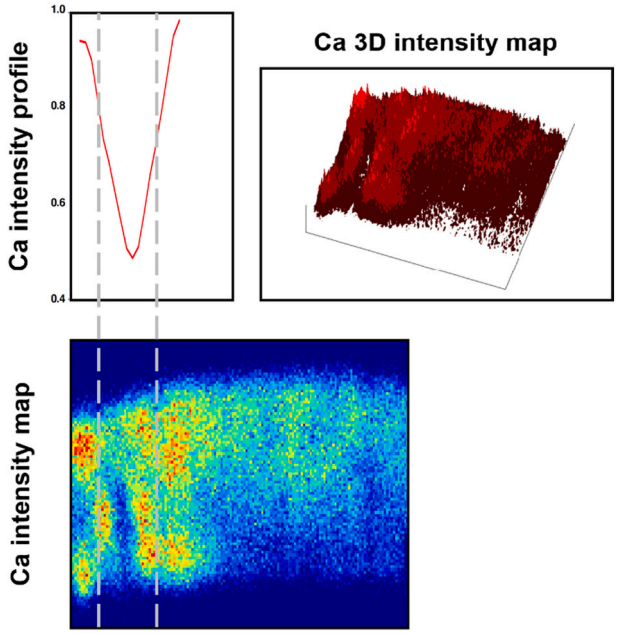

Fig. 14. Normalized intensity profile of calcium and 3D intensity map.

TORNADO. It is possible to reduce the acquisition time for the FF-XRF system with some changes to the experimental setup, such as the use of different optical components (e.g., multi-hole collimators).

In conclusion, the applicability of the FF-XRF imaging system based on the 2D-THCOBRA for studies related to heavy metal accumulation on biological samples was shown, being capable of detecting reduced amounts of these metals. Moreover, the system has shown to be advantageous for quick preliminary assessments of bioaccumulation.

CRediT authorship contribution statement

F.D. Leite: Data curation, Formal analysis, Writing – original draft, Writing – review & editing. **P.M.S. Carvalho:** Data curation, Formal analysis, Writing – original draft, Writing – review & editing. **R.G. Oliveira:** Software. **M.C. Lopes:** Data curation, Software. **I. Domingues:** Supervision, Resources, Writing – review & editing. **P.M.M. Correia:** Methodology, Writing – review & editing. **L.F.N.D. Carramate:** Methodology, Writing – review & editing. **S. Pessanha:** Conceptualization, Methodology, Resources, Writing – review & editing. **J.F.C.A. Veloso:** Conceptualization, Methodology, Funding acquisition. **A.L.M. Silva:** Supervision, Conceptualization, Methodology, Funding acquisition, Writing – original draft, Writing – review & editing.

Declaration of Competing Interest

None.

Data availability

Data will be made available on request.

Acknowledgements

This work was partially supported by projects PTDC/FIS-AQM/32536/2017, CERN/FIS-INS/0026/2019 and STRONG-2020–824093 through FCT and H2020 programs. It was also developed within the scope of the i3N (UIDB/50025/2020 & UIDP/50025/2020) and CESAM (UIDP/50017/2020 & UIDB/50017/2020 & LA/P/0094/2020), financed by national funds through the FCT/MEC COMPETE, FEDER and POCI programs.

The costs resulting from the FCT (Fundação para a Ciência e a Tecnologia, I.P–Portuguese Foundation for Science and Technology) hiring L.F.N.D. Carramate were funded by national funds (OE) in the scope of the framework contract CEECIND/01369/2017, and S. Pessanha in the scope of the framework contract CEECIND/00278/2018.

F.D. Leite is grateful for the grant BII/UI96/9175/2020, R.G. Oliveira is grateful for the grant SFRH/BI/10638/2020, and P.M.S. Carvalho is grateful to FCT for the PhD grant PD/BD/128324/2017.

References

[1] M.A. Zoroddu, J. Aaseth, G. Crisponi, S. Medici, M. Peana, V.M. Nurchi, The essential metals for humans: a brief overview, J. Inorg. Biochem. 195 (2019) 120–129, https://doi.org/10.1016/j.jinorgbio.2019.03.013.
[2] A.L. Wani, A. Ara, J.A. Usmani, Lead toxicity: a review, Interdiscip. Toxicol. 8 (2) (Jun. 2015) 55, https://doi.org/10.1515/INTOX-2015-0009.
[3] L. Järup, Hazards of heavy metal contamination, Br. Med. Bull. 68 (2003) 167–182, https://doi.org/10.1093/bmb/ldg032.
[4] WHO, Exposure to Arsenic: A Major Public Health Concern, 2019.
[5] S.L. O'Neal, W. Zheng, Manganese toxicity upon overexposure: a decade in review, Curr. Environ. Heal. Rep. 2 (3) (2015) 315–328, https://doi.org/10.1007/S40572-015-0056-X.
[6] S. Rivera-Mancía, C. Ríos, S. Montes, Manganese accumulation in the CNS and associated pathologies, BioMetals 24 (5) (Oct. 2011) 811–825, https://doi.org/10.1007/S10534-011-9454-1/FIGURES/1.
[7] M. Hason, P. Bartůněk, Zebrafish models of cancer-new insights on modeling human cancer in a non-mammalian vertebrate, Genes (Basel) 10 (11) (2019) 1–30, https://doi.org/10.3390/genes10110935.
[8] I. Domingues, R. Oliveira, J. Lourenço, C.K. Grisolia, S. Mendo, A.M.V.M. Soares, Biomarkers as a tool to assess effects of chromium (VI): comparison of responses in zebrafish early life stages and adults, Comp. Biochem. Physiol. - C Toxicol. Pharmacol. 152 (3) (2010) 338–345, https://doi.org/10.1016/j.cbpc.2010.05.010.
[9] A.P. Singh, C. Nüsslein-Volhard, Zebrafish stripes as a model for vertebrate colour pattern formation, Curr. Biol. 25 (2) (2015) R81–R92, https://doi.org/10.1016/j.cub.2014.11.013.
[10] K. Howe, et al., The zebrafish reference genome sequence and its relationship to the human genome, Nature 496 (7446) (2013) 498–503, https://doi.org/10.1038/nature12111.
[11] A.L. Menke, J.M. Spitsbergen, A.P.M. Wolterbeek, R.A. Woutersen, Normal anatomy and histology of the adult zebrafish, Toxicol. Pathol. 39 (5) (2011) 759–775, https://doi.org/10.1177/0192623311409597.
[12] M.L. Carvalho, S. Santiago, M.L. Nunes, Assessment of the essential element and heavy metal content of edible fish muscle, Anal. Bioanal. Chem. 382 (2) (2005) 426–432, https://doi.org/10.1007/s00216-004-3005-3.
[13] F. Bilo, et al., Total reflection X-ray fluorescence spectroscopy to study Pb and Zn accumulation in zebrafish embryos, X-Ray Spectrom. 44 (2015) 124–128, https://doi.org/10.1002/xrs.2588.
[14] M. Korbas, S.R. Blechinger, P.H. Krone, I.J. Pickering, G.N. George, Localizing organomercury uptake and accumulation in zebrafish larvae at the tissue and cellular level, Proc. Natl. Acad. Sci. U. S. A. 105 (34) (2008) 12108–12112, https://doi.org/10.1073/pnas.0803147105.
[15] R.G. Leitao, M.P. Silva, M.S. Diniz, M. Guerra, Mapping the distribution of mercury (II) chloride in zebrafish organs by benchtop micro-energy dispersive X-ray fluorescence : a proof of concept, J. Trace Elem. Med. Biol. 69 (2022), https://doi.org/10.1016/j.jtemb.2021.126874.
[16] P.M.S. Carvalho, et al., Elemental mapping of Portuguese ceramic pieces with a full-field XRF scanner based on a 2D-THCOBRA detector, Eur. Phys. J. Plus 136 (4) (2021), https://doi.org/10.1140/epjp/s13360-021-01422-y.
[17] P.O. Onuwa, L.A. Nnamonu, I.S. Eneji, R. Sha'Ato, Analysis of heavy metals in human scalp hair using energy dispersive X-ray fluorescence technique, J. Anal. Sci. Methods Instrum. 02 (04) (2012) 187–193, https://doi.org/10.4236/jasmi.2012.24029.
[18] P.M.S. Carvalho, et al., Energy dispersive X-ray fluorescence quantitative analysis of biological samples with the external standard method, Spectrochim. Acta - Part B At. Spectrosc. 174 (2020) 105991, https://doi.org/10.1016/j.sab.2020.105991, no. October.
[19] A.L.M. Silva, R. Figueroa, A. Jaramillo, M.L. Carvalho, J.F.C.A. Veloso, Performance of a gaseous detector based energy dispersive X-ray fluorescence imaging system: analysis of human teeth treated with dental amalgam, Spectrochim Acta - Part B At. Spectrosc. 86 (2013) 115–122, https://doi.org/10.1016/j.sab.2013.03.005.
[20] M4 TORNADO. https://www.bruker.com/en/products-and-solutions/elemental-analyzers/micro-xrf-spectrometers/m4-tornado.html.
[21] J. Žemlička, J. Jakůbek, M. Kroupa, V. Tichý, Energy- and position-sensitive pixel detector Timepix for X-ray fluorescence imaging, Nucl. Instruments Methods Phys. Res. Sect. A Accel. Spectrometers, Detect. Assoc. Equip. 607 (1) (Aug. 2009) 202–204, https://doi.org/10.1016/J.NIMA.2009.03.140.
[22] A.L.M. Silva, et al., Elemental mapping in a contemporary miniature by full-field X-ray fluorescence imaging with gaseous detector vs. scanning X-ray fluorescence imaging with polycapillary optics, Spectrochim. Acta - Part B At. Spectrosc. 129 (2017) 1–7, https://doi.org/10.1016/j.sab.2016.12.006.
[23] J.F.C.A. Veloso, A.L.M. Silva, Gaseous detectors for energy dispersive X-ray fluorescence analysis, Nucl. Instruments Methods Phys. Res. Sect. A Accel.

Spectrometers, Detect. Assoc. Equip 878 (2018) 24–39, https://doi.org/10.1016/j.nima.2017.09.011. September 2017.
[24] M. Alfeld, K. Janssens, A. Sasov, The use of full-field XRF for simultaneous elemental mapping, AIP Conf. Proc. 1221 (2010) 111–118, https://doi.org/10.1063/1.3399236.
[25] P.M.S. Carvalho, et al., Elemental mapping of Portuguese ceramic pieces with a full-field XRF scanner based on a 2D-THCOBRA detector, Eur. Phys. J. Plus 136 (4) (2021), https://doi.org/10.1140/epjp/s13360-021-01422-y.
[26] S. Altenhofen, M.T. Wiprich, L.R. Nery, C.E. Leite, M.R.M.R. Vianna, C.D. Bonan, Manganese(II) chloride alters behavioral and neurochemical parameters in larvae and adult zebrafish, Aquat. Toxicol. 182 (2017) 172–183, https://doi.org/10.1016/j.aquatox.2016.11.013.
[27] N.V. Dolgova, et al., Distribution of selenium in zebrafish larvae after exposure to organic and inorganic selenium forms, Metallomics 8 (3) (2016) 305–312, https://doi.org/10.1039/c5mt00279f.
[28] C.B. Singh, B.A. Ansari, Toxicity of two heavy metals Lead and cobalt on zebrafish, Danio rerio, Sch. Acad. J. Biosci. (SAJB) 5 (9) (2017) 682–687, https://doi.org/10.21276/sajb.2017.5.9.17.
[29] F.D. Amaro, C. Santos, J.F.C.A. Veloso, A. Breskin, R. Chechik, J.M.F. Dos Santos, The thick-COBRA: a new gaseous electron multiplier for radiation detectors, J. Instrum. 5 (10) (Oct. 2010), https://doi.org/10.1088/1748-0221/5/10/P10002.
[30] A.L.M. Silva, et al., X-ray imaging detector based on a position sensitive THCOBRA with resistive line, J. Instrum. 8 (5) (2013), https://doi.org/10.1088/1748-0221/8/05/P05016.
[31] L.F.N.D. Carramate, A.L.M. Silva, C.D.R. Azevedo, D.S. Covita, J.F.C.A. Veloso, THCOBRA X-ray imaging detector operating in Ne/CH4, J. Instrum. 10 (1) (2015), https://doi.org/10.1088/1748-0221/10/01/P01003.
[32] A.L.M. Silva, R. Figueroa, A. Jaramillo, M.L. Carvalho, J.F.C.A. Veloso, 'Performance of a gaseous detector based energy dispersive X-ray fluorescence imaging system: analysis of human teeth treated with dental amalgam', *Spectrochim*, Acta - Part B At. Spectrosc. 86 (2013) 115–122, https://doi.org/10.1016/j.sab.2013.03.005.
[33] S. Pessanha, A. Samouco, R. Adão, M.L. Carvalho, J.P. Santos, P. Amaro, Detection limits evaluation of a portable energy dispersive X-ray fluorescence setup using different filter combinations, X-Ray Spectrom. 46 (2) (Mar. 2017) 102–106, https://doi.org/10.1002/XRS.2737.
[34] S.L. O'Neal, W. Zheng, Manganese toxicity upon overexposure: a decade in review, Curr. Environ. Heal. Rep. 2 (3) (2015) 315–328, https://doi.org/10.1007/S40572-015-0056-X.
[35] G. Robison, et al., X-ray fluorescence imaging: a new tool for studying manganese neurotoxicity, PLoS One 7 (11) (2012) 48899, https://doi.org/10.1371/JOURNAL.PONE.0048899.
[36] S. Bakthavatsalam, S. Das Sharma, M. Sonawane, V. Thirumalai, A. Datta, A zebrafish model of manganism reveals reversible and treatable symptoms that are independent of neurotoxicity, DMM Dis. Model. Mech. 7 (11) (2014) 1239–1251, https://doi.org/10.1242/dmm.016683.
[37] R.C. Balachandran, et al., Brain manganese and the balance between essential roles and neurotoxicity, J. Biol. Chem. 295 (19) (2020) 6312–6329, https://doi.org/10.1074/JBC.REV119.009453.
[38] K. Tuschl, et al., Mutations in SLC39A14 disrupt manganese homeostasis and cause childhood-onset parkinsonism–dystonia, Nat. Commun. 7 (2016), https://doi.org/10.1038/ncomms11601.
[39] S.F. da Silva, D.C. Oliveira, J.P.G. Pereira, S.P. Castro, B.N.S. Costa, M. De O. Lima, Seasonal variation of mercury in commercial fishes of the Amazon triple frontier, Western Amazon Basin, Ecol. Indic. 106 (Nov. 2019), 105549, https://doi.org/10.1016/J.ECOLIND.2019.105549.
[40] WHO, Selenium in Drinking-Water, 2011.
[41] S. Choudhury, et al., Selenium preferentially accumulates in the eye Lens following embryonic exposure: a confocal X-ray fluorescence imaging study, Environ. Sci. Technol. 49 (4) (2015) 2255–2261, https://doi.org/10.1021/es503848s.
[42] Lead poisining. https://www.who.int/news-room/fact-sheets/detail/lead-poisoning-and-health, 2021 (accessed Dec. 26, 2021).
[43] N.H.B. Thi, et al., Chronic exposure to low concentration lead chloride-induced anxiety and loss of aggression and memory in zebrafish, Int. J. Mol. Sci. 21 (5) (2020) 1844, https://doi.org/10.3390/ijms21051844.
[44] J. Chen, et al., Developmental lead acetate exposure induces embryonic toxicity and memory deficit in adult zebrafish, Neurotoxicol. Teratol. 34 (6) (2012) 581–586, https://doi.org/10.1016/j.ntt.2012.09.001.
[45] C. Rice, J.K. Ghorai, K. Zalewski, D.N. Weber, Developmental lead exposure causes startle response deficits in zebrafish, Aquat. Toxicol. 105 (3–4) (Oct. 2011) 600–608, https://doi.org/10.1016/J.AQUATOX.2011.08.014.
[46] Y. Zhang, J. Feng, Y. Gao, X. Liu, L. Qu, L. Zhu, Physiologically based toxicokinetic and toxicodynamic (PBTK-TD) modelling of Cd and Pb exposure in adult zebrafish Danio rerio: accumulation and toxicity, Environ. Pollut. 249 (Jun. 2019) 959–968, https://doi.org/10.1016/J.ENVPOL.2019.03.115.